

Multiple Microalterations Detected at High Frequency in Oral Cancer

Corisande Baldwin,^{1,2} Cathie Garnis,^{1,2} Lewei Zhang,³ Miriam P. Rosin,¹ and Wan L. Lam^{1,2}

¹British Columbia Cancer Research Centre, and Departments of ²Pathology and Laboratory Medicine and ³Oral Biological and Medical Sciences, University of British Columbia, Vancouver, British Columbia, Canada

Abstract

The development of array comparative genomic hybridization (array CGH) at tiling-path resolution has enabled the detection of gene-sized segmental DNA copy number gains and losses. Here, we present the first application of whole genome tiling-path array CGH to archival clinical specimens for the detailed analysis of oral squamous cell carcinomas (OSCC). We describe the genomes of 20 OSCCs as well as a selection of matched normal DNA in unprecedented detail. Examination of their whole genome profiles enabled the identification of alterations ranging in size from whole-arm, segmental, to gene size alterations. Tiling-path resolution enabled the detection of many more alterations within each tumor than previously reported, many of which include narrow alterations found to be frequent events among the 20 OSCCs. We report the presence of several novel frequent submegabase alterations, such as the 0.58 Mb gain at 5p15.2 containing triple functional domain (*TRIO*), detected in 45% of cases. We also report the first coamplification of two gene clusters, by fine-mapping the precise base pair boundaries of the high-level amplification at 11q22.2-22.3 containing both matrix metalloproteinase and baculoviral IAP repeat-containing protein 2 (*BIRC*) gene clusters. These results show the large improvement in detection sensitivity and resolution compared with genome interval marker arrays and the utility of tiling resolution array CGH for the detection of both submegabase and single copy gains and losses in cancer gene discovery. (Cancer Res 2005; 65(17): 7561-7)

Introduction

Oral cancer is the most common head and neck neoplasm, affecting >400,000 people worldwide each year.⁴ The prevention and management of this disease will greatly benefit from the identification of molecular markers and targets (1, 2). Frequent loss of heterozygosity or recurrent segmental DNA copy number changes are indicative of chromosomal regions containing genes critical to tumorigenesis. Array comparative genomic hybridization (array CGH) enables the detection of segmental gains and losses of DNA. We previously reported the application of this technology to identify genetic alterations on chromosome arm 3p in oral carcinoma (3). The recent development of a bacterial artificial chromosome (BAC) tiling-path array that spans the human genome with 32,433 overlapping clones has made the analysis of the entire genome possible at unprecedented resolution (4), revealing both

large-scale as well as gene-size alterations, which are not visible using conventional megabase interval genome-wide array CGH analysis such as that described by Snijders et al. (5). Here, we present the first application of whole genome tiling-path array CGH to clinical specimens for the detailed analysis of oral squamous cell carcinoma (OSCC) genomes in order to identify numerous novel frequent submegabase alterations.

Materials and Methods

Tissue samples. Formalin-fixed paraffin-embedded OSCCs were obtained from the British Columbia Oral Biopsy Service and diagnoses confirmed by an oral pathologist (L. Zhang). Tumor cells were micro-dissected and DNA was extracted and quantified as previously described (6). Clinical information and demographics for these cases are presented in Supplementary Table S1.

Whole genome tiling-path array CGH analysis. The whole genome array contains 97,299 elements, representing 32,433 BAC-derived amplified fragment pools spotted in triplicate and randomly distributed throughout two microarray slides (4). The ability to detect single copy changes is confirmed as part of the quality control of array production. This involves hybridization of normal male versus normal female DNA and examination of the X chromosome profiles to control for detection sensitivity of single copy change as previously described (4).

Sample and reference (normal diploid male) genomic DNA (400 ng each) was random prime labeled with 4 nmol of cyanine-3 and cyanine-5 dCTP, respectively. Purified samples were hybridized and washed as previously described (3). Spot images were captured and analyzed using an Arrayworx scanner and SoftWorx Tracker Spot Analysis software (Applied Precision, Issaquah, WA). SeeGH custom software was used to visualize all data as log₂ ratio plots (7). This software is available publicly online.⁵ Clones with SDs between triplicate spots >0.075 or with signal-to-noise ratios of <10 were stringently filtered from the raw data.

Genetic alterations and their associated breakpoints were identified using both aCGH-Smooth software (8) and visual analysis. The aCGH-Smooth software package identifies copy number gains and losses using a local search algorithm that calculates the probability that the signal ratio for each BAC clone corresponds with the same copy number status as a set of nearby clones using maximum likelihood estimation (8). Visual analysis of the normalized data in SeeGH by multiple karyogram alignment was employed to confirm alterations identified by aCGH-Smooth and to define minimal regions. In order to avoid false-positives due to hybridization "noise," a minimum of two consecutive clones showing change was required for a region to be considered altered. This was made possible by the overlapping coverage of the tiling-path array.

Results and Discussion

Tiling-path array CGH characterizes genetic alterations. Complete SeeGH karyograms were generated for 24 microdissected archival specimens including 20 OSCCs and 4 matched normal connective tissues. Each karyogram summarizes copy number status for the 32,433 DNA segments providing a global view of these

Note: Supplementary data for this article are available at Cancer Research Online (<http://cancerres.aacrjournals.org/>).

Requests for reprints: Corisande Baldwin, British Columbia Cancer Research Centre, 675 West 10th Avenue, Vancouver, British Columbia, Canada, V5Z 1L3. Phone: 604-675-8112; Fax: 604-675-8185; E-mail: cbaldwin@bccrc.ca.

©2005 American Association for Cancer Research.
doi:10.1158/0008-5472.CAN-05-1513

⁴ http://www3.who.int/whosis/discussion_papers/pdf/papers13.pdf

⁵ <http://www.flintbox.ca/technology.asp?tech=FB312FB>

tumor genomes. Many regions of alteration previously detected with conventional metaphase CGH were found in these profiles (9, 10). Both gross chromosomal aberrations as well as specific regional changes are apparent. Figure 1A presents the SeeGH karyogram of one tumor, 125T, with the remainder given as supplemental data online.⁶ In this profile, we observed alterations such as loss on 3p and 9p, two of the early genetic changes known to OSCC (11). The karyogram also revealed small and complex alterations. For example, chromosome 11 exhibits large regions of copy number loss on the long arm (11q), a gain encompassing 11q13.3 (*Cyclin D1*), and a small high copy number gain 11q22.2-22.3 (*MMP* cluster) as well as the breakpoint of a deletion at the telomere of 11p (Fig. 1B). The details seen in this example illustrate the value of the enhanced resolution provided by the tiling-path array.

To confirm the reliability of the whole genome array, we compared array CGH data from this study against those from our previous work. One tumor, 528T, previously analyzed using the 535 clone 3p-arm specific array (3), was compared with the 3p data generated by the whole genome array (with 957 clones covering 3p). Although only 104 clones were common between the two arrays, the two profiles are identical, illustrating the robustness of the array CGH approach (Fig. 1C).

Frequency plot analysis to identify recurring alterations. To facilitate the identification of regions of frequent gain or loss, a frequency plot of the genetic alterations at each of the 32,000 loci among the 20 OSCC samples was constructed (Fig. 2A). Generation of this frequency plot required first the use of a CGH-Smooth software to identify segmental imbalances in each genomic profile (see legend of Fig. 2), followed by frequency calculation and data display using SeeGH software version 2.2.2. In order to identify recurrent changes and to define minimal regions of alteration, frequently altered regions identified in the frequency plot were then confirmed in a multiple alignment analysis to verify the presence of these alterations in the original data.

Interestingly, the whole genome tiling-path array detected many more alterations in the OSCCs than previously reported using conventional techniques. For example, the total number of gains and losses detected with aCGH-Smooth in 125T was 312, consisting of 100 deletions and 212 gains. In contrast, reports in the literature for total number of alterations in oral tumors using conventional CGH have yielded values <20 (9, 10), whereas reports using interval marker array CGH have only focused on rare amplicons. The increased detection sensitivity in our study can be attributed to the high resolution of the tiling-path array. The 10- to 15-fold increase in clone coverage over interval arrays (5) resulted in the identification of small submegabase genetic alterations that may have otherwise escaped detection.

As shown in Fig. 2A, the frequency of alteration is nonrandom. Certain chromosome arms are mostly gained, whereas others are mostly lost. Overall, copy number deletions seem to be more common than copy number gains. A variety of frequent alterations are evident, many of which correspond to known regions of chromosomal aberration. For example, chromosome arm 3p seems to be the most frequently lost region followed by $\geq 50\%$ loss on 4, 5q, 8p, 9p, 10q, 11, 18q, and 21q. Conversely, the most frequently gained regions seem to be 8q followed by 3q, with smaller regions on 9q, 11q (*CCND1*), 14q, and 20q. Although some chromosomes show concurrent frequent gain and loss, these

alterations may be attributed to genomic instability rather than a selective mechanism. Interestingly, whereas losses often affect entire chromosome arms, gained regions tend to be segmental (Fig. 2A). The frequency plot shows various "peaks" corresponding to segmental copy gains, for example, 11q and 12p. At tiling resolution, the frequency plot identifies common alterations that may be missed by conventional CGH.

Defining anticipated alterations in OSCC. To show the sensitivity of the tiling array, we confirmed the presence of copy number changes known to be frequent in OSCC using SeeGH karyogram alignment. This allowed both the identification of minimal regions of alteration and the establishment of the precise boundaries of copy number change for each region.

Multiple alignment of the tiling-path data at 7p11.2, which harbors *EGFR* in all 20 OSCCs allowed the identification of a 1.06 Mb minimal region of copy number gain present in 8 of 20 cases (40%), which is consistent with previous studies using array CGH (ref. 12; Fig. 2B). This shows a large improvement in the detection sensitivity and resolution compared with interval arrays which reportedly detected a low frequency of copy number gain present in just 4 of 89 tumors (5%; ref. 5). Figure 2B shows the alignment of three cases at 7p11.2 (161T, 793T, and 528T) illustrating segmental alteration that differs in both the width and level of gain. The minimal region spans from clone RP11-16407 to RP11-535N12 and contains only five annotated genes including *EGFR*.

In another example, Fig. 2C shows three cases with gain at the *Cyclin D1* locus at 11q13.3, again demonstrating a variance in both the width and level of copy number increase. This gain was frequent as shown by the peak at 11q13 in the frequency plot, present in 9 of 20 (45%) cases with high copy number amplifications in 7 cases. The 0.79 Mb amplicon defined by case 125T in Fig. 2C encompasses eight genes including *Cyclin D1*.

Multiple alignment of chromosome arm 8p data showed two neighboring minimal regions of copy number loss at 8p23.2 [from BAC clone CTD-2042C19 to RP11-234C5 (0.19 Mb), and from RP11-567H20 to RP11-315I17 (0.32 Mb)]. Loss on 8p23 has been previously reported (13). Both regions were present at equal frequency of 13 of 20 (65%) cases. Examination of 8p23.2 on the human genome map revealed that a single 2.06 Mb gene, CUB Sushi domain 1 (*CSMD1*), spans both regions and is, therefore, interrupted by deletion. Interestingly, three cases show a narrow copy number decrease that appears within an apparent whole arm loss suggesting that loss of *CSMD1* may represent a homozygous loss in these cases. Two of these cases (125T and 528T) are shown in Fig. 2D. *CSMD1* encodes a transmembrane protein that has been previously identified as lost in head and neck squamous cell carcinoma, and often by homozygous deletion (13). This region also shows the sensitivity of our array to detect single copy changes.

Novel frequent regions of segmental alteration. In addition to these known regions, we also detected many frequent novel alterations. These alterations include copy number gains at 3q23, 5p15.2, 7p12.3-13, 7q21.2, and 7q35 and copy number losses at 2p15, 4q34.3, and 16q23.2. All regions were submegabase in size and were present in as few as 7, and as many as 15, of the 20 cases. These regions are listed in Supplementary Table S2 available online⁶ and may also represent alterations critical to oral tumorigenesis.

Figure 3A and B show two contrasting examples of copy number gains detected using the tiling-path array. First, a novel submegabase segmental gain was detected at 7q35 in 8 of 20 cases (40%). Samples 125T, 123T, and 486T each showed an amplified region containing a single gene, rho guanine nucleotide exchange factor 5

⁶ http://www.bccrc.ca/cg/ArrayCGH_Group.html

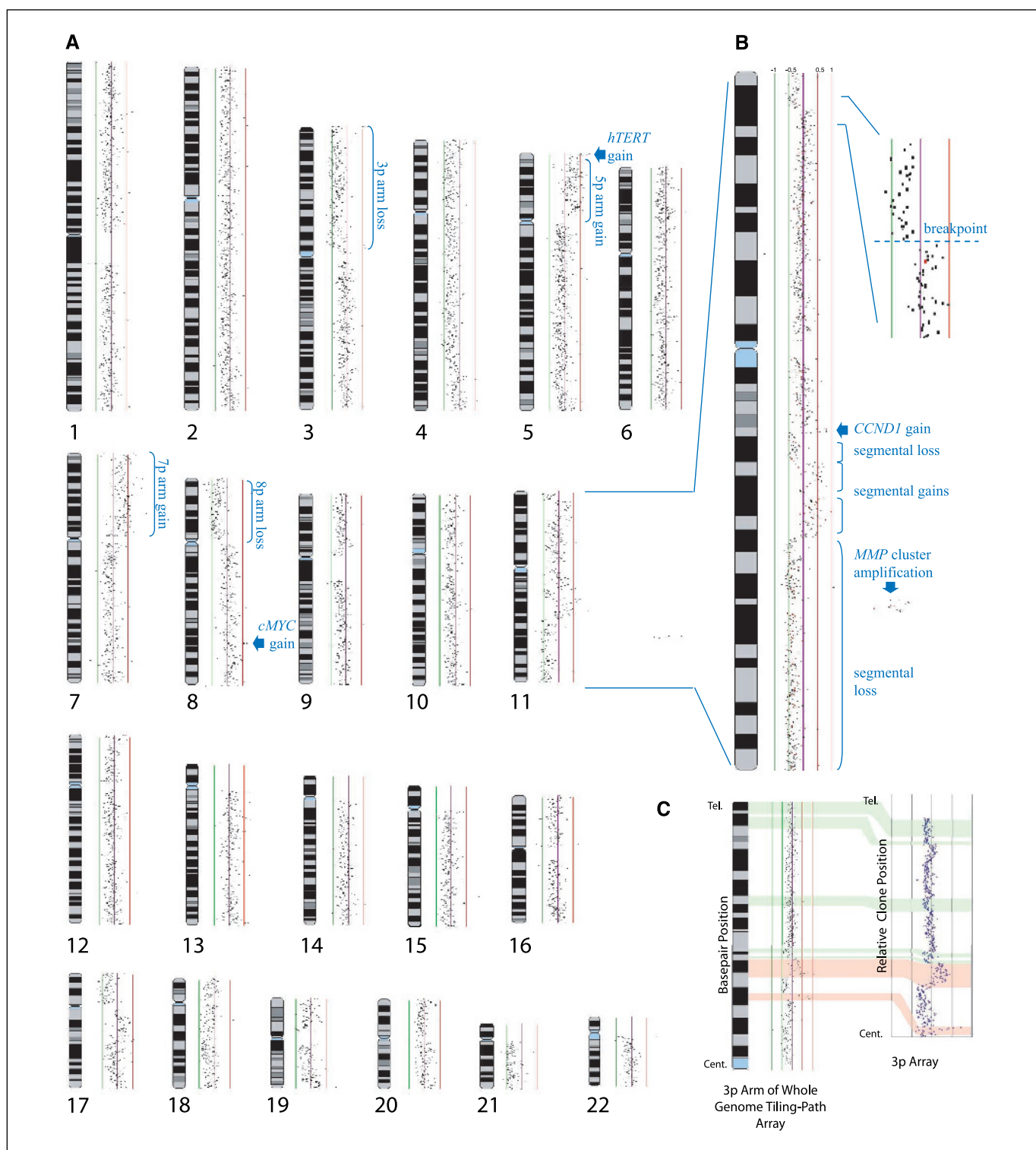


Figure 1. High-resolution SeeGH karyogram analysis of oral tumors. **A**, whole genome karyogram of tumor 125T. SeeGH software was used to plot the \log_2 signal intensity ratios of tumor versus reference DNA at each BAC clone. Each dot represents the signal ratio for an individual BAC clone. The green and red lines are scale bars indicating \log_2 signal intensity ratios of +0.5 and -0.5, respectively. Multiple regions of copy number gain (5p and 7p) and loss (3p and 8p) are apparent, with the array revealing small and/or complex alterations. We also see gains at the *hTERT* (5p15.33) and *cMYC* (8q24.21) loci. **B**, small and complex alterations on chromosome 11 show the sensitivity of the array to detect detailed alterations, both high copy number and single copy number changes. Chromosome 11 exhibits multiple genetic alterations on both arms. Large regions of segmental copy number loss and segmental gain are evident. Magnification of these segmental changes enables the identification of the precise location of breakpoints between neighboring BAC clones. Multiple focal changes such as a gain at 11q13.3 (containing *CCND1*) and a small novel high copy number gain 11q22.2-22.3 (*MMP* cluster) are also detected. **C**, comparison of 3p profiles of tumor 528T shows the robustness of the whole genome tiling-path array. These profiles were generated from the whole genome tiling-path array (3p data, 957 overlapping clones plotted according to base pair positions) in the current work (left) and the previously published 3p-specific array, which consisted of 535 clones plotted in relative clone order (right, ref. 3). Although only 104 clones are common between these arrays, identical regions of alteration were identified. Examples are shaded green and red.

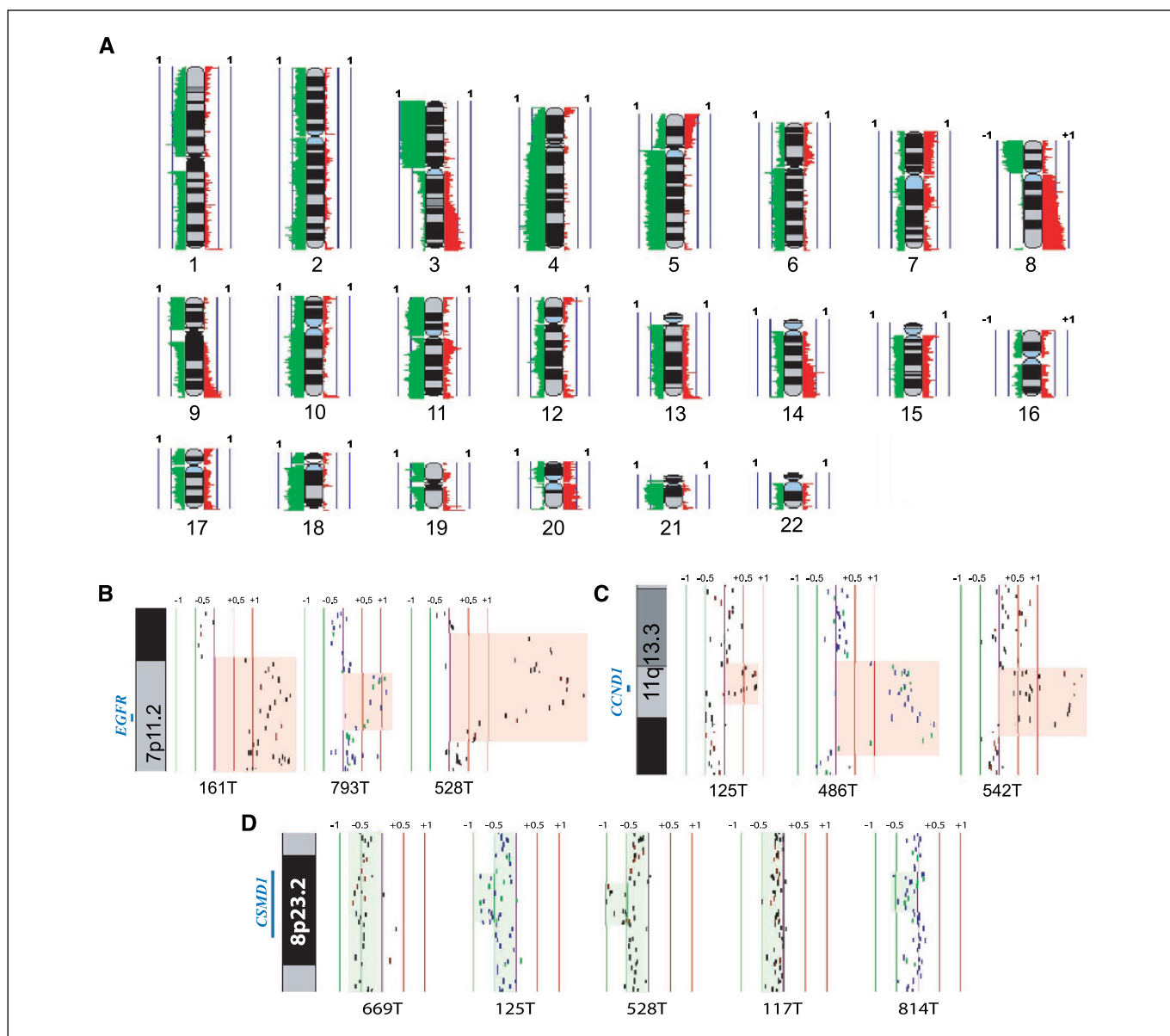


Figure 2. Frequency of gains and losses. *A*, summary of frequency of losses (green, left) and gains (red, right) detected by aCGH-Smooth software for each chromosome arm. The bars to the left and right of the chromosomes represent a frequency of 0.5 and 1, respectively. The aCGH-Smooth software identifies alterations and their associated breakpoints in the normalized data by employing a local search algorithm. By calculating the probability that a given clone is of the same copy number status as a set of previous clones, the algorithm calculates a maximum likelihood for each clone. This enables the identification of putative breakpoints which are then shifted randomly upstream and downstream to calculate an overall goodness of fit (8). Thus, groups of clones considered to have the same copy number status are assigned a relative value. Gains and losses for each clone were then tabulated for 20 OSCCs and plotted in SeeGH software (7) to generate a frequency plot for the identification of “hotspots” or regions of frequent gain and loss. *B*, alignment of three cases (161T, 793T, and 528T) showing gains (red) at 7p11.2 (*EGFR* locus) that differ in both width and level. The central bar and the red bars to the right and green bars to the left, represent \log_2 signal intensity ratios of 0, +0.5 and +1, and -0.5 and -1 , respectively, between the sample and reference DNA. *C*, alignment of three cases (125T, 486T, and 542T) showing a gain at 11q13.3, *CCND1* locus (red). *D*, alignment of losses at 8p23.2 in 5 cases (669T, 125T, 528T, 117T, 814T) with the deleted region shaded in green disrupting the 2.06 Mb *CSMD1* gene.

(*ARHGEF5*). One case (486T) showed a high-level amplification that was absent in the matched non-cancer DNA derived from underlying connective tissue (Fig. 3A). *ARHGEF5* is a member of the Dbl guanine nucleotide exchange factor family specific for Rho GTPases, which are well-known to be involved in tumorigenesis (14).

Second, and most noticeable, a 2.17-Mb-wide high copy gain at 11q22.2-22.3 was detected in two samples (125T and 805T) with a single copy number gain in an additional sample (628T; Fig. 3B). The extremely high copy number amplification at this region

suggests its biological importance. A recent study on OSCC using a genome-wide interval marker array reported a rare amplicon (5.6% of cases) at this loci. However, here we report a much higher frequency (15%) and have fine-mapped the breakpoints in greater detail. In fact, the region we describe here contains 17 known genes, with two gene clusters, including nine matrix metalloproteinase (*MMP*) genes (*MMPI*, 3, 7, 8, 10, 12, 13, 20, and 27), and two baculoviral IAP repeat-containing protein (*BIRC*) genes (*BIRC2* and 3). This is the first report of the coamplification of two

gene clusters, both relevant to oral cancer. *BIRC2* and *BIRC3* are known to function in inhibition of apoptosis and have been shown to be amplified in lung cancer (15). *MMP* gene products function in invasion and metastasis through degradation of the basement membrane and extracellular matrix. *MMP* overexpression has previously been associated with oral cancer (16).

Frequent amplification and overexpression of *TRIO*. Multiple karyogram alignment of the 5p arm revealed a novel 0.58 Mb copy number gain at 5p15.2 present in 9 of 20 cases. Figure 4A shows the alignment of three such cases (125T, 161T, and 486T) showing the most narrow segmental gains detected at this region. The region spanning from RP11-744A15 to RP11-611H4, encompasses a single known gene, triple functional domain (*TRIO*), and is not seen in the matched normal samples. *TRIO* expression was significantly higher in the four OSCCs compared with the seven normal specimens (Fig. 4A). *TRIO* contains three functional domains—a serine/threonine kinase domain and two guanine exchange factor domains. *TRIO* amplification and abundant expression was recently reported in lung carcinoma and bladder cancer (17–19). Although 5p amplifications have been well -documented in oral cancer, this is the first report of the microamplification of the *TRIO* locus in oral cancer, probably due to insufficient resolution of both conventional techniques and interval marker array CGH.

Frequent amplification and overexpression of *CDK6*. Multiple karyogram alignment of the 7q arm revealed a 0.32 Mb copy

number gain at 7q21.2 present in 6 of 20 cases. Although a “rare” 3 Mb amplicon has been previously described (5), we detected this region with much higher frequency (30%) and have fine-mapped precise breakpoints at RP11-82E23 and at RP11-514K1. The minimal region we describe encompasses two known genes, cyclin-dependent kinase 6 (*CDK6*) and peroxisome biogenesis factor 1 (*PEX1*). Figure 4B shows the alignment of three cases that exhibited the most narrow copy number gains (528T, 542T, and 486T). *CDK6* has been shown to be overexpressed in numerous squamous cell carcinoma cell lines including OSCC cell lines (20), and is well known to positively regulate the cell cycle, emphasizing its potential role in oral tumorigenesis. In contrast, *PEX1* functions in peroxisomal matrix protein import, which, if interrupted, results in peroxisomal biogenesis disorders and has not previously been implicated in tumorigenesis. Therefore, only *CDK6* was further investigated. *CDK6* expression was evaluated in four tumors and seven normal specimens—the same samples used in comparing *TRIO* expression. As shown, *CDK6* expression was significantly higher in the tumors compared with the normal sample sets (Fig. 4B). Deregulation of *TRIO* and *CDK6* at the transcriptional level shows the biological significance of these loci.

Conclusion. In this study, we presented the first application of whole genome tiling-path array CGH to clinical specimens. We interrogated 32,433 overlapping segments covering the genome for the detailed delineation of the genomic landscapes of 20 OSCCs.

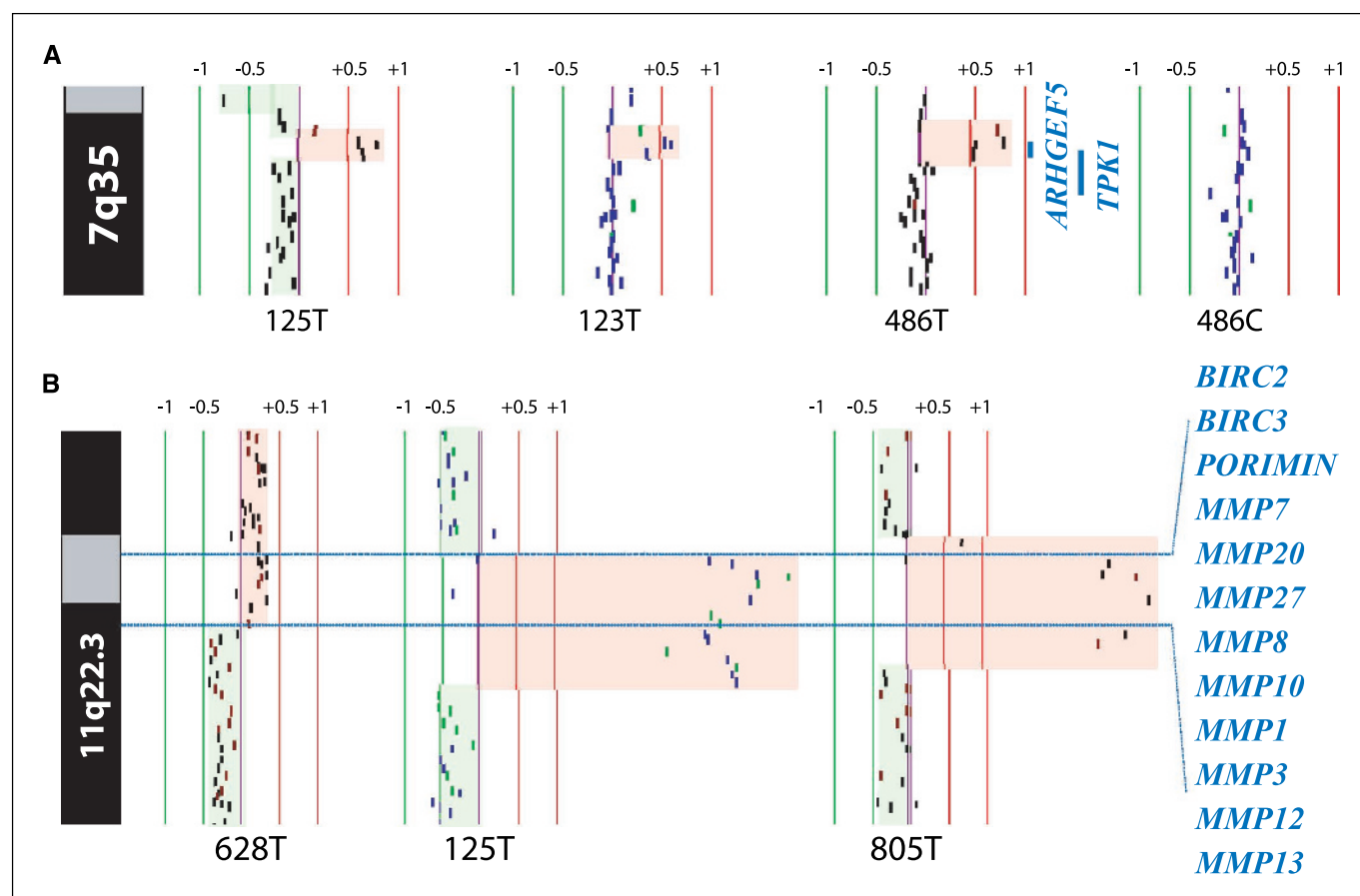


Figure 3. Novel regions of segmental gain. *A*, alignment of 125T, 123T, and 486T, shows a novel submegabase gain at 7q35, unchanged in matched normal sample (486C) corresponding to 486T. Shaded red areas, copy number gain. Shaded green areas, losses; see legend of Fig. 2B for further explanation on ratio bars. The high level gain present in tumor 486T is absent in the matched normal. *B*, high level amplification at 11q22.2-22.3. Minimal region of alteration is marked by dashed lines and contains a cluster of 12 genes including 9 *MMP* genes and 2 *BIRC* genes (right).

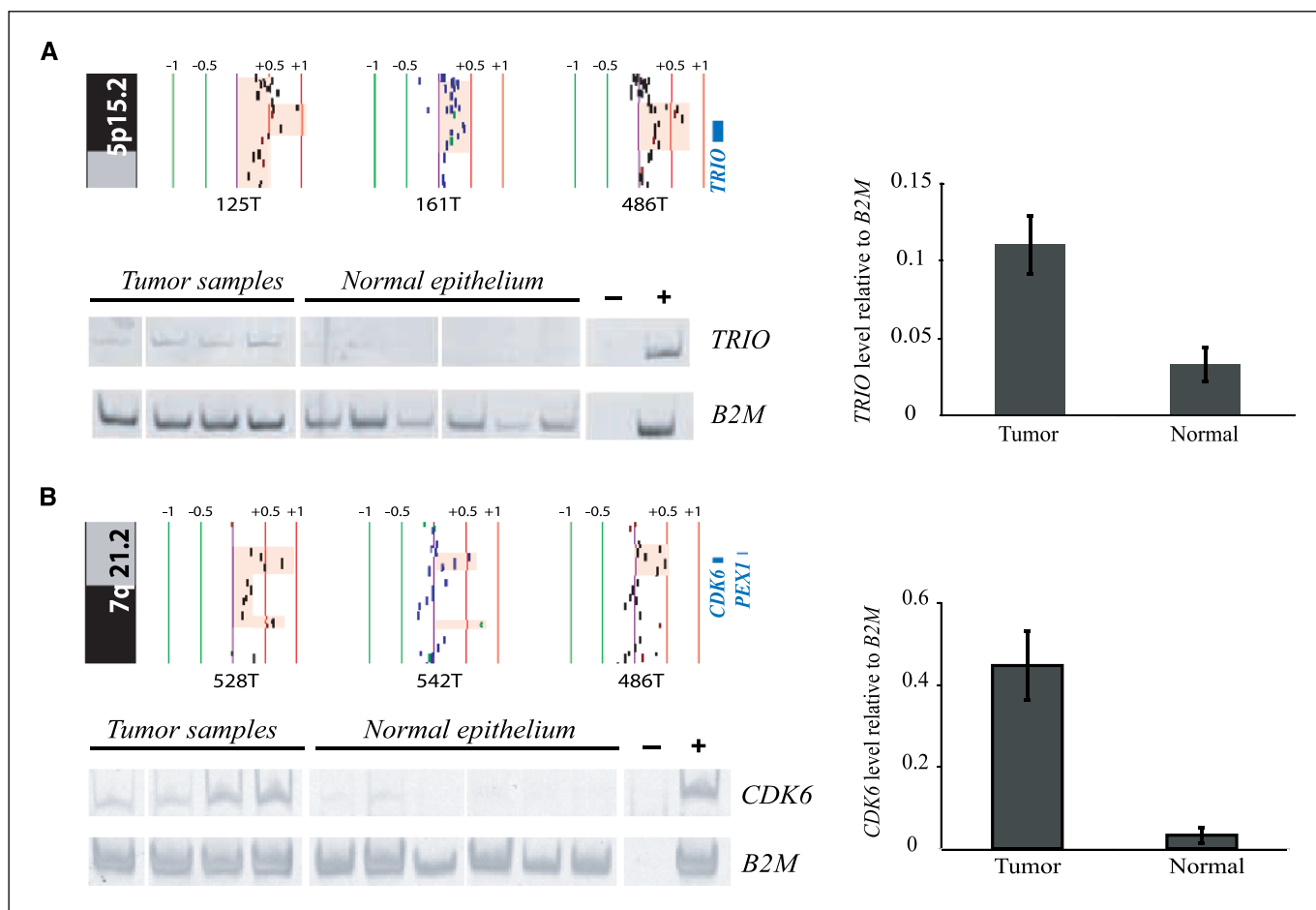


Figure 4. Novel gains at the *TRIO* and *CDK6* regions. **A**, alignment of 125T, 161T, and 486T, which show a gain at 5p15.2, with the unchanged matched normal sample (486C) corresponding to 486T. Genomic regions of gain are shaded (red). Location of *TRIO* is denoted in blue (right); see legend of Fig. 2B for further explanation on ratio bars. *TRIO* transcript levels were compared in four microdissected frozen OSCC and six normal samples by RT-PCR. Histograms show average expression level of *TRIO* in relation to that of β 2-microglobulin in both tumors and normal, with the corresponding SE in each group. Statistical significance of the differences between tumors and normals was determined using the Mann-Whitney *U* test with a *P* = 0.05. **B**, alignment of 528T, 542T, and 486T showing a novel 0.32 Mb region of gain which is absent in the matched normal sample 486C. Genomic regions of gain are shaded (red). This region was present in 6 of 20 cases and encompasses two known genes, *CDK6* and *PEX1*. Location of *CDK6* and *PEX1* is denoted in blue (right). *CDK6* transcript levels were compared as described in (A).

This unprecedented resolution enabled analysis from the whole genome view, to individual chromosome arm views, and down to the gene level. At this resolution, we showed the presence of numerous genetic alterations common in OSCC too diminutive for detection by conventional cytogenetic techniques. The detection of submegabase segmental amplifications at 5p15.2, containing *TRIO*, at 7q21.2, containing *CDK6*, and at 11q22.2-22.3, containing the *MMP* gene cluster are prime examples. These results validate the need to employ tiling resolution analysis of tumor genomes in cancer gene-discovery.

Acknowledgments

Received 5/2/2005; revised 6/28/2005; accepted 7/6/2005.

Grant support: National Institute of Dental and Craniofacial Research grants R01 DE13124 and R01 DE015965; Canadian Institute of Health Research; Genome Canada/British Columbia; the Hardwick scholarship (C. Baldwin); the National Science Engineering Research Council (C. Garnis) and the Michael Smith Foundation for Health Research scholarships (C. Garnis).

The costs of publication of this article were defrayed in part by the payment of page charges. This article must therefore be hereby marked *advertisement* in accordance with 18 U.S.C. Section 1734 solely to indicate this fact.

We thank S. Watson, C. Malloff, R. DeLeeuw, B. Chi, P. Wang, J. Davies, and B. Coe for array synthesis and bioinformatics assistance.

References

- Sabichi AL, Demierre MF, Hawk ET, Lerman CE, Lippman SM. Frontiers in cancer prevention research. *Cancer Res* 2003;63:5649-55.
- Spafford MF, Koch WM, Reed AL, et al. Detection of head and neck squamous cell carcinoma among exfoliated oral mucosal cells by microsatellite analysis. *Clin Cancer Res* 2001;7:607-12.
- Garnis C, Baldwin C, Zhang L, Rosin MP, Lam WL. Use of complete coverage array comparative genomic hybridization to define copy number alterations on chromosome 3p in oral squamous cell carcinomas. *Cancer Res* 2003;63:8582-5.
- Ishkanian AS, Malloff CA, Watson SK, et al. A tiling resolution DNA microarray with complete coverage of the human genome. *Nat Genet* 2004;36:299-303.
- Snijders AM, Schmidt BL, Fridlyand J, et al. Rare amplicons implicate frequent deregulation of cell fate specification pathways in oral squamous cell carcinoma. *Oncogene* 2005;24:4232-42.
- Zhang L, Michelsen C, Cheng X, Zeng T, Priddy R, Rosin MP. Molecular analysis of oral lichen planus. A premalignant lesion? *Am J Pathol* 1997;151:323-7.
- Chi B, DeLeeuw RJ, Coe BP, MacAulay C, Lam WL.

- SeeGH—a software tool for visualization of whole genome array comparative genomic hybridization data. *BMC Bioinformatics* 2004;5:13.
8. Jong K, Marchiori E, Meijer G, Van Der Vaart A, Ylstra B. Breakpoint identification and smoothing of array comparative genomic hybridization data. *Bioinformatics* 2004;20:3636–7.
9. Squire JA, Bayani J, Luk C, et al. Molecular cytogenetic analysis of head and neck squamous cell carcinoma: by comparative genomic hybridization, spectral karyotyping, and expression array analysis. *Head Neck* 2002;24:874–87.
10. Tremmel SC, Gotte K, Popp S, et al. Intratumoral genomic heterogeneity in advanced head and neck cancer detected by comparative genomic hybridization. *Cancer Genet Cytogenet* 2003;144:165–74.
11. Mao L, Hong WK, Papadimitrakopoulou VA. Focus on head and neck cancer. *Cancer Cell* 2004;5:311–6.
12. Garnis C, Campbell J, Zhang L, Rosin MP, Lam WL, OCGR array: an oral cancer genomic regional array for comparative genomic hybridization analysis. *Oral Oncol* 2004;40:511–9.
13. Toomes C, Jackson A, Maguire K, et al. The presence of multiple regions of homozygous deletion at the CSMD1 locus in oral squamous cell carcinoma question the role of CSMD1 in head and neck carcinogenesis. *Genes Chromosomes Cancer* 2003;37:132–40.
14. Debily MA, Camarca A, Ciullo M, et al. Expression and molecular characterization of alternative transcripts of the ARHGEF5/TIM oncogene specific for human breast cancer. *Hum Mol Genet* 2004;13:323–34.
15. Dai Z, Zhu WG, Morrison CD, et al. A comprehensive search for DNA amplification in lung cancer identifies inhibitors of apoptosis cIAP1 and cIAP2 as candidate oncogenes. *Hum Mol Genet* 2003;12:791–801.
16. Lin SC, Lo SS, Liu CJ, Chung MY, Huang JW, Chang KW. Functional genotype in matrix metalloproteinases-2 promoter is a risk factor for oral carcinogenesis. *J Oral Pathol Med* 2004;33:405–9.
17. Coe BP, Henderson LJ, Garnis C, et al. High-resolution chromosome arm 5p array CGH analysis of small cell lung carcinoma cell lines. *Genes Chromosomes Cancer* 2005;42:308–13.
18. Zheng M, Simon R, Mirlacher M, et al. TRIO amplification and abundant mRNA expression is associated with invasive tumor growth and rapid tumor cell proliferation in urinary bladder cancer. *Am J Pathol* 2004;165:63–9.
19. Garnis C, Davies JJ, Buys TP, et al. Chromosome 5p aberrations are early events in lung cancer: implication of glial cell line-derived neurotrophic factor in disease progression. *Oncogene* 2005;24:4806–12.
20. Timmermann S, Hinds PW, Munger K. Re-expression of endogenous p16ink4a in oral squamous cell carcinoma lines by 5-aza-2'-deoxycytidine treatment induces a senescence-like state. *Oncogene* 1998;17:3445–53.

Cancer Research

The Journal of Cancer Research (1916–1930) | The American Journal of Cancer (1931–1940)

Multiple Microalterations Detected at High Frequency in Oral Cancer

Corisande Baldwin, Cathie Garnis, Lewei Zhang, et al.

Cancer Res 2005;65:7561-7567.

Updated version Access the most recent version of this article at:
<http://cancerres.aacrjournals.org/content/65/17/7561>

Supplementary Material Access the most recent supplemental material at:
<http://cancerres.aacrjournals.org/content/suppl/2005/08/29/65.17.7561.DC1>

Cited articles This article cites 20 articles, 6 of which you can access for free at:
<http://cancerres.aacrjournals.org/content/65/17/7561.full#ref-list-1>

Citing articles This article has been cited by 20 HighWire-hosted articles. Access the articles at:
<http://cancerres.aacrjournals.org/content/65/17/7561.full#related-urls>

E-mail alerts [Sign up to receive free email-alerts](#) related to this article or journal.

Reprints and Subscriptions To order reprints of this article or to subscribe to the journal, contact the AACR Publications Department at pubs@aacr.org.

Permissions To request permission to re-use all or part of this article, contact the AACR Publications Department at permissions@aacr.org.